Regionalization of Seasonal Precipitation over the Tibetan Plateau and Associated Large-Scale Atmospheric Systems

HUI-WEN LAI,[a] HANS W. CHEN,[b] JULIA KUKULIES,[a] TINGHAI OU,[a] AND DELIANG CHEN[a]

[a] Department of Earth Sciences, University of Gothenburg, Gothenburg, Sweden
[b] Department of Physical Geography and Ecosystem Science, Lund University, Lund, Sweden

(Manuscript received 10 July 2020, in final form 10 December 2020)

ABSTRACT: Precipitation over the Tibetan Plateau (TP) has major societal impacts in South and East Asia, but its spatiotemporal variations are not well understood, mainly because of the sparsely distributed in situ observation sites. With the help of the Global Precipitation Measurement satellite product IMERG and the ERA5 dataset, distinct precipitation seasonality features over the TP were objectively classified using a self-organizing map algorithm fed with 10-day averaged precipitation from 2000 to 2019. The classification reveals three main precipitation regimes with distinct seasonality of precipitation: the winter peak, centered at the western plateau; the early summer peak, found on the eastern plateau; and the late summer peak, mainly located on the southwestern plateau. On a year-to-year basis, the winter peak regime is relatively robust, whereas the early summer and late summer peak regimes tend to shift mainly between the central and northern TP but are robust in the eastern and southwestern TP. A composite analysis shows that the winter peak regime experiences larger amounts of precipitation in winter and early spring when the westerly jet is anomalously strong to the north of the TP. Precipitation variations in the late summer peak regime are associated with intensity changes in the South Asian high and Indian summer monsoon. The precipitation in the early summer peak regime is correlated with the Indian summer monsoon together with anticyclonic circulation over the western North Pacific. The results provide a basic understanding of precipitation seasonality variations over the TP and associated large-scale conditions.

KEYWORDS: Asia; Large-scale motions; Precipitation; Satellite observations; Classification; Monsoons

1. Introduction

The Tibetan Plateau (TP)—often considered as the ''Third Pole''—is the world's largest and highest plateau as well as the origin of most major rivers that provide water resources to countries in South and East Asia (Immerzeel et al. 2020). Over the recent decades, the TP has experienced amplified warming compared with the rest of the globe, similar to the enhanced warming in the Arctic (Liu and Chen 2000; Chen et al. 2015; Bibi et al. 2018; Yao et al. 2019). Moreover, the warming rate over the TP is larger at higher elevations than at lower elevations (Liu et al. 2009). The TP is also becoming wetter with increases in water vapor content and precipitation (Xu et al. 2008; Yang et al. 2011). However, the precipitation changes are heterogeneous in space with decreases at some locations (Bibi et al. 2018). Understanding the spatiotemporal variability in precipitation over the plateau thus plays an important role in water management for downstream societies.

The seasonality of precipitation over the TP is influenced by many large-scale atmospheric systems, such as Asian monsoons (e.g., Wang et al. 2001; Yim et al. 2014), midlatitude westerlies (e.g., Schiemann et al. 2009), and subtropical highs (e.g., Zhang et al. 2004; X. Zhang et al. 2018). Compared with other regions at similar Northern Hemisphere latitudes, the TP acts as a huge heat source to the atmosphere in summer, which can affect the stability and induce atmospheric circulations that are crucial for the regional climate and weather (Flohn 1957; Yeh 1957; Yanai et al. 1992; Yanai and Tomita 1998; Ye and Wu 1998; Yanai and Wu 2006). For example, the thermal and dynamical effects of the plateau influence the Asian monsoon circulations and may alter variabilities of monsoon precipitation (Wang and LinHo 2002; Zhang et al. 2015), including the monsoon onset, downstream rainfall, and moisture convergence (Park et al. 2012).

It is well established that summer monsoons contribute the most to the precipitation over the TP (Xu et al. 2008; Feng and Zhou 2012; Maussion et al. 2014; Xu et al. 2020). The rainband of Asian summer monsoons starts from the Bay of Bengal and the South China Sea in mid-May, moves northward to the southeastern TP in early June, and reaches the southwestern TP in mid-July. The monsoon cycles are responsible for the spatiotemporal shift of monsoon rainfall peak over the TP and adjacent regions (Tanaka 1992; Zhang et al. 2004). Based on different spatiotemporal characteristics of rainfall peak, the Asian summer monsoon can be generally divided into three monsoon subsystems with different spatiotemporal peaks of precipitation: the Indian summer monsoon (ISM), the western North Pacific summer monsoon (WNPSM), and the East Asian summer monsoon (EASM) (Wang and LinHo 2002; Ding and Chan 2005).

Subtropical highs and westerly jet streams also play an important role in the TP precipitation. For example, the South Asian high and western North Pacific subtropical high interact with monsoons and westerlies, affecting precipitation in the region. Particularly, the moving of the monsoon rainband is

Denotes content that is immediately available upon publication as open access.

Corresponding author: Deliang Chen, deliang@gvc.gu.se

DOI: 10.1175/JCLI-D-20-0521.1

modulated by the strength and location of the western North Pacific subtropical high (Chang et al. 2000; Lau et al. 2000; Huang et al. 2018), while interannual variations in the South Asian high influence the ISM and EASM rainfall intensity (Wei et al. 2019). In addition, the migrations of the subtropical westerly jet and diabatic heating due to summertime radiative heating over the TP were found to lead to changes in the onset of monsoon precipitation (Sato 2009; Ge et al. 2017). The subtropical westerly jets also influence winter precipitation over the western and southern TP. For example, the meridional position of the subtropical westerly jet was found to influence the amount and the location of precipitation of the TP (Schiemann et al. 2009).

The moisture supplies to the TP are affected by changes in Rossby wave trains crossing Eurasia, monsoon circulation, and surface temperatures (Bothe et al. 2010; Zhang et al. 2017). For example, the moisture transports from the west of the TP by the midlatitude westerlies and from the southwest by the ISM have likely contributed the most moisture to the precipitation over the northwestern TP (Zhang et al. 2017). Warming temperatures could enhance the frequencies of changes and shifts in the summer monsoon (Zhang et al. 2017). Therefore, understanding the associated large-scale flows and their variability is crucial to study the interannual variations of precipitation over the TP.

It is often useful to distinguish different climate regimes when studying regional climate variations. The most well-known climate regime classification is the Köppen climate classification, which can be used to diagnose climate change and identify regions that are more sensitive to climate change (Chen and Chen 2013). The Köppen climate classification usually uses monthly climatologically averaged temperature and precipitation to identify different climate types. However, because of the high elevation of the TP and cold biases in many datasets over the plateau (e.g., Orsolini et al. 2019; Zhu and Yang 2020), the entire TP is often classified as tundra climate, which is not useful to separate different precipitation regimes. Further, the use of a global classification to a specific region such as the TP may bring an inherent limitation. A number of studies have therefore attempted to classify the precipitation regimes over the TP based on other criteria. Using stable oxygen isotope measurements at a limited number of sites, Yao et al. (2013) suggested that the TP can be divided into three zones with distinct seasonal precipitation cycles: the southern and northern regions are controlled by the Asian summer monsoons and westerlies, respectively, while the region in between is considered a transition zone. This north–south-oriented division of the TP has guided many following studies (e.g., Kukulies et al. 2019). However, due to the limited observational sites, especially in the western and northern TP, and the proxy nature of the isotopes for precipitation, the boundaries between different precipitation regimes could not be precisely determined. Indeed, several studies using in situ observations, reanalyses, and satellite data have found a division along the northwest–southeast direction rather than the north–south orientation for the spatial distribution of seasonal precipitation over the TP, although there are still disagreements about the main mechanisms behind the seasonality in precipitation (You et al. 2015; Zhu and Sang 2018; Kukulies et al. 2020).

So far, the only systematic classification of the precipitation seasonality over the TP was done with the help of dynamic downscaling driven by an earlier global analysis (Curio and Scherer 2016). The monthly downscaled precipitation, covering a period during 2001–13, helped resolve the issue that there is a lack of information in the central and western parts of the TP, and was used to classify the intraseasonal characteristics of monthly precipitation in the High Asia Refined analysis using K-means clustering. The analysis revealed a westerly dominant, monsoon dominant, and convective activity dominant regime, as well as several regimes that were affected by interactions between the above-mentioned systems. However, the data period of this study is relatively short, and the data used did not cover the whole TP. Perhaps more importantly, this and other previous studies have focused on characterizing the stationary precipitation regimes over the TP; however, the robustness of regimes and shifts in regimes over time have so far been mostly neglected. Furthermore, to what extent different regions in the TP are controlled by which atmospheric large-scale systems has not been clearly explained. A reasonable and physically meaningful explanation can be particularly useful to interpret future circulation changes from climate model projections and to understand what implications these have on precipitation regimes.

With the help of recently available high-resolution satellite data and a state-of-the-art high-resolution global reanalysis, this study attempts to overcome some of the limitations encountered by the previous studies and to provide a regionalization of the TP based on its seasonal precipitation characteristics, as well as investigate what atmospheric systems are mainly associated with these different seasonal precipitation regimes. We will present a new objective precipitation classification over the TP based on the seasonality of precipitation derived from two independent sources, and explore the variabilities of precipitation induced by different types of atmospheric systems. Specifically, we aim to 1) identify regions with different distinct seasonality in precipitation, 2) determine the interannual variability in the classification and regional precipitation, and 3) explore the roles played by large-scale atmospheric circulations on the seasonality of regional precipitation. The results from the precipitation regionalization will lead to a better understanding of the boundaries and interannual variations of precipitation regimes over the TP, and may help to interpret future changes in precipitation regimes due to climate change.

2. Data and methods

This study takes advantage of the newly available satellite data from the Global Precipitation Measurement (GPM), high-resolution ERA5, as well as ground-based measurements from the China Meteorological Administration (CMA) and NOAA's Global Historical Climatology Network (GHCN), to characterize the seasonality and interannual variations of precipitation over the TP.

a. ERA5 and observational precipitation dataset

In this study, we focus on the domain of 25°–45°N, 65°–105°E, which covers the main plateau with an elevation over 3000 m and adjacent areas. The precipitation data used are hourly and monthly precipitation from ERA5, half-hourly precipitation from GPM, and daily in situ precipitation provided by CMA and GHCN.

ERA5 is the fifth generation of atmospheric reanalyses provided by the European Centre for Medium-Range Weather Forecasts (Hersbach et al. 2018), featuring hourly estimates of atmospheric variables at a horizontal resolution of about 31 km globally. For the classification we used hourly precipitation from ERA5, including both the accumulated rain and snow, on a $0.25° \times 0.25°$ grid and covering the period June 2000–May 2019 to be consistent with the GPM data. To study the atmospheric conditions, we used ERA5 monthly averaged data from 1979 to 2019, including precipitation, mean sea level pressure (MSLP), geopotential height at 300 hPa (GPH300), the u component of the wind at 300 and 850 hPa, the v component of the wind at 850 hPa, and the vertical integral of eastward and northward water vapor fluxes.

To evaluate the performance of the precipitation data in the reanalysis, we also performed the classification using satellite observations. For this analysis, we used gauge-calibrated half-hourly precipitation estimates from the Integrated Multi-satellite Retrievals for GPM (IMERG) Level-3 product (version 06) at a spatial resolution of 0.1° over the period June 2000–May 2019. This satellite product combines data from various microwave and IR satellite sensors (Hou et al. 2014). Previous studies have shown that GPM IMERG reduces the precipitation biases over the TP in comparison to other data products (Xu et al. 2017; S. Zhang et al. 2018). Additionally, the new version of GPM IMERG has the advantage of a homogenous GPM–TRMM calibration, resulting in precipitation estimates that encompass 20 years instead of 5 years from the previous version.

The classification was furthermore verified using in situ daily precipitation from the CMA and GHCN over the period June 2000–May 2018. Because the in situ data were not consistently collected from all stations through time, we selected a subset of stations that covered at least 60% of the whole time period, resulting in a total of 413 stations.

b. Classification

All precipitation data were averaged to 10-day averages starting from 1 June each year, resulting in 37 values per year (with the last value being a 5-day average, leap days omitted). Given that the seasonal cycle is the dominant signal, the results are relatively insensitive to the choice of averaging time window. We chose 10-day averages to smooth out some of the noisy daily variability while at the same preserving a higher temporal resolution than monthly averages. We define a year from June to May to make the most use of the GPM data, which are available from June 2000. The classification was performed on the seasonal cycles of precipitation represented by these 37 values for each grid point and year. To avoid having a few grid points with large precipitation amounts dominate the classification, the precipitation data were standardized before the analysis by subtracting the annual mean of 10-day averaged precipitation and dividing by the standard deviation of annual 10-day averaged precipitation for each grid point and year.

A neural network algorithm called a self-organizing map (SOM) was applied to the precipitation data to identify subregions in the TP and adjacent regions with similar seasonality of precipitation. SOM is a machine learning process for organizing similar data into clusters (Kohonen 1982). The SOM algorithm is performed in two phases: training and mapping. During the training phase, SOM uses unsupervised learning to reduce a high-dimensional dataset to a low-dimensional map of nodes that represent different characteristics of the original dataset. After the map has been created, any data point can be mapped to the nodes by finding the node on the map with the closest Euclidean distance to the data point. The SOM method is similar to principal component analysis and K-means clustering, which are regularly used in climate research. However, unlike principal component analysis, SOM is capable of nonlinear mappings and does not impose orthogonality between the factors of variability. A major difference between SOM and K-means clustering is that SOM nodes are connected to adjacent nodes by a neighborhood function, which preserves the topology of the original data. These features make SOMs useful for reducing high-dimensional data into a low-dimensional space, typically in two dimensions for easy visualization (Mwasiagi 2011).

Here we applied the SOM training on annual cycles of standardized 10-day averaged precipitation from ERA5 and GPM during the period June 2000–May 2019. Thus, the sample size is the number of domain grid points $\times$ 19 years. We then used the trained SOMs to classify the 19-yr mean seasonal cycles of standardized precipitation from ERA5 and GPM, 18-yr mean seasonal cycles from in situ observations, and the seasonal cycles for each year during the 19-yr period for all datasets. The ERA5 and GPM classifications were trained separately and used to classify their own precipitation data. Because the majority of the in situ observations are concentrated in the eastern TP and are scarce in the central and western TP, we did not train a SOM using the in situ data, but instead mapped the in situ observations using the ERA5 and GPM trained SOMs to verify the classification results.

The classification results are influenced by the size of the SOM grid. To determine the optimal SOM size, we applied the elbow method (Thorndike 1953), which considers the sum of squared Euclidean distances between the input data points and the respective closest matching node. When the number of nodes increases, the sum of squared Euclidean distances decreases. The idea is to choose a number where adding new nodes does not significantly decrease the sum of squared Euclidean distances. We tested several grid sizes (from 2×2 to 9×9) for each classification algorithm, and determined that a total number of 20 (4×5) nodes was sufficient to capture the variability in the data. This SOM size resulted in several superfluous transition nodes with small cluster sizes. To simplify the analysis and focus on large-scale features, we merged some clusters based on the similarity between their nodes. First, we selected clusters that occupy more than 1/20 of the total area of the domain, denoted as leading clusters. Leading clusters that shared more than 95% of their variance with another leading cluster were merged into the larger cluster. Next, we calculated the correlation coefficients between the nodes of the leading clusters and all other clusters. The other clusters were merged with the respective leading cluster that shares the highest correlation.

c. *Composite analysis of large-scale circulation*

After identifying subregions with distinct seasonality in precipitation, we applied composite analysis to identify large-scale atmospheric systems associated with the interannual precipitation variations for each subregion. For this analysis, we used the monthly mean estimates from ERA5 over 1979–2019. First, we identified grid points whose yearly seasonal cycles of precipitation were consistently classified to the same cluster at least 80% over 2000–19, which we denoted as robust regions. Then, we defined a rainy season for each robust region as the months when the precipitation exceeds the annual mean. Time series (1979–2019) of spatially and seasonally averaged precipitation were calculated and detrended for the rainy seasons for each robust region. Finally, we selected for each robust region the 10 years with the largest precipitation amounts and the 10 years with the smallest precipitation amounts, denoted as wet years and dry years.

Atmospheric conditions associated with regional precipitation were examined by constructing composite averages of meteorological fields in the rainy seasons during wet and dry years. We focus on meteorological variables that can represent large-scale systems from low to high altitudes. Following previous studies, we examined the westerlies around the TP by analyzing the geopotential height above 500 hPa (Schiemann et al. 2009; Cannon et al. 2016; Mölg et al. 2017). The South Asian high, which is one of the important systems affecting monsoon circulations, is also commonly studied at about 500 hPa (Flohn 1957; Yeh 1957). Because the surface height of the TP is close to 500 hPa, we chose the u wind at 300 hPa and GPH300 to study the high-level atmosphere. Wang et al. (2008) summarized that most of the studies apply sea level pressure and u and v winds to define monsoon circulations. Therefore, we chose the MSLP, u wind at 850 hPa, and v wind at 850 hPa to study monsoon circulations outside the plateau. Finally, we also examined moisture fluxes to investigate the moisture transport for precipitation. All atmospheric fields were detrended prior to the composite analysis. Student's t test was used to determine if the composites of dynamical factors are statistically significant.

3. Regional seasonality

a. *Averaged seasonality of precipitation classification*

Figure 1 shows the trained SOM of seasonal cycles of standardized precipitation from GPM, as well as the 19-yr mean data points from GPM that were mapped to the different clusters. Each data point corresponds to a grid point in the dataset. The node in the upper-left corner of the SOM grid represents grid points with a relatively flat seasonal cycle of precipitation and most of the precipitation occurring in winter and early spring. The grid points mapped to the bottom-left node experience less precipitation in winter and more precipitation between May and August. The bottom-right node shows a sharp peak in precipitation around the end of July and the beginning of August, while the upper-right node shows a small peak in August and a larger peak in September. Some data points have a precipitation peak in December that is not captured well by any of the SOM nodes, likely because this feature is overshadowed by the summer precipitation variability. The nodes between the corner nodes show a transition between these different regimes of seasonal precipitation over the TP and adjacent regions. The SOM trained using ERA5 data shows a similar structure (not shown). For most clusters, the average correlation coefficient between the data points and corresponding representative nodes is above 0.7, which shows that the SOM classification captures well the spatiotemporal distribution of precipitation in this domain. There are four clusters with correlation coefficients below 0.7. These clusters do not have many data points mapped to them and represent transitions between the main nodes.

Figures 2a and 2b show the spatial distribution of the 20 SOM clusters for the 19-yr averaged seasonal cycles of precipitation from ERA5 and GPM, respectively. The two datasets were used to train two SOMs independently and mapped to the clusters of their respective SOM. The classifications of in situ precipitation (circles in Figs. 2c,d) agree well with the clustering results from ERA5 and GPM. The time series of standardized 10-day precipitation anomalies (Figs. 2e,f) from ERA5 and GPM show that a major part of the annual precipitation fell between May and September in the clusters located at the northern, eastern, and southern plateau. In contrast, most of the annual precipitation in the western plateau occurred in winter and early spring. Generally, the SOM clusters show a west-to-east distribution, reflecting the different seasonal timing of precipitation.

Figures 2e and 2f show that many clusters share similar characteristics of seasonal precipitation with some minor differences. To simplify the classification and focus on the influences from systems on the synoptic scale and on time scales ranging from weeks to months, the 20 clusters were regrouped into three leading precipitation regimes based on the correlation coefficients among the SOM nodes (see section 2b). Figures 3a and 3b display the distribution of the three regimes for the 19-yr average seasonal cycles of precipitation. The three precipitation regimes are centered at the western, southwestern, and eastern plateau; the clear east–west spatial distribution of seasonal precipitation agrees well with the findings of You et al. (2015), Curio and Scherer (2016), and Kukulies et al. (2020). The western plateau has a dominant contribution of precipitation in winter and early spring (winter peak regime) and covers eastern Kyrgyzstan, eastern Tajikistan, and northern Pakistan. The southwestern plateau and northern India form a region with a dominant contribution of precipitation

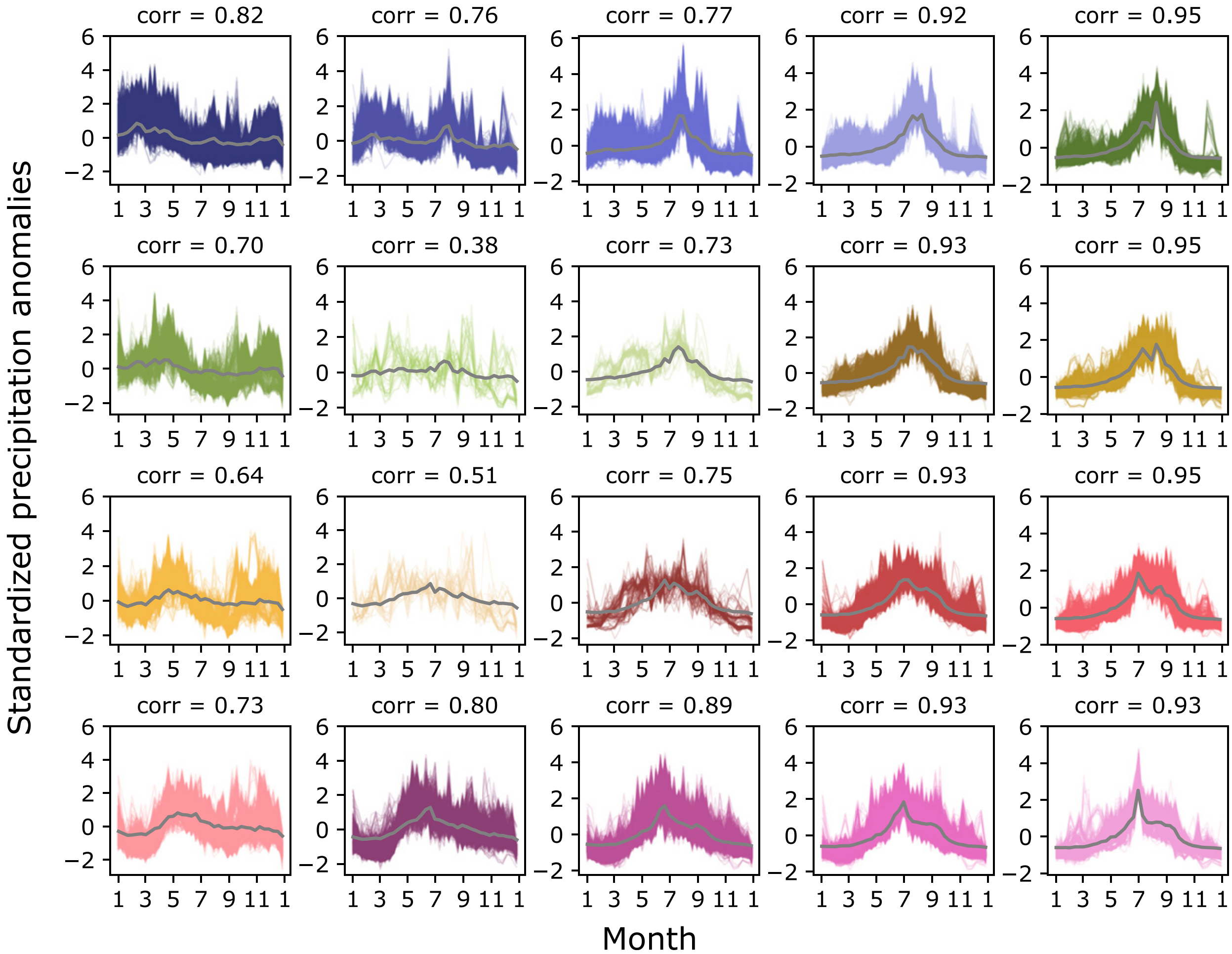

FIG. 1. The 4 × 5 SOM clusters of standardized seasonal precipitation anomalies from GPM. The gray lines show the trained SOM nodes, and the colored lines show the 19-yr mean seasonal cycles of standardized precipitation data points that were mapped to each node. The number above each cluster denotes the average correlation coefficient between the data points and the representative node in each cluster.

mainly from July to August (late summer peak regime). The eastern plateau region, with a maximum contribution of precipitation in June (early summer peak regime), covers the northern and southeastern plateau as well as northern Qinghai–Tibet where the elevation is lower than 3000 m. A small portion of the eastern domain is also classified as being part of the late summer peak regime. The spatiotemporal characteristics of these three clusters show the distinctive seasonality of precipitation in different areas within the study domain.

Classified in situ observations according to the three leading precipitation regimes agree well with the classification using ERA5 and GPM data (Figs. 3c,d), with 84% of the observations matching the ERA5 classification and 88% matching the GPM classification. Most of the mismatches between ERA5/GPM and in situ classifications are found at the boundaries between regimes, such as in the southeastern, central, and northwestern TP. The mismatches are likely due to local-scale variations of precipitation that are not captured well in the ERA5 dataset and satellite-derived GPM product.

The precipitation classifications from ERA5 and GPM are overall consistent with each other in terms of spatial distribution and seasonal cycle characteristics of precipitation regimes. The major differences between the ERA5 and GPM classifications are found at the boundaries between the early summer and late summer peak regimes over the north-central plateau. The results of the classification with ERA5 are similar to those with GPM as well as in situ observations, and show that the ERA5 precipitation could be valuable for studying the climatology of precipitation over the TP.

b. *Interannual variation of regional precipitation classification*

To examine the interannual variations and long-term changes of the three precipitation regimes and boundaries between regimes, we performed the classification on each year from June 2000 to May 2019, resulting in 19 classification maps

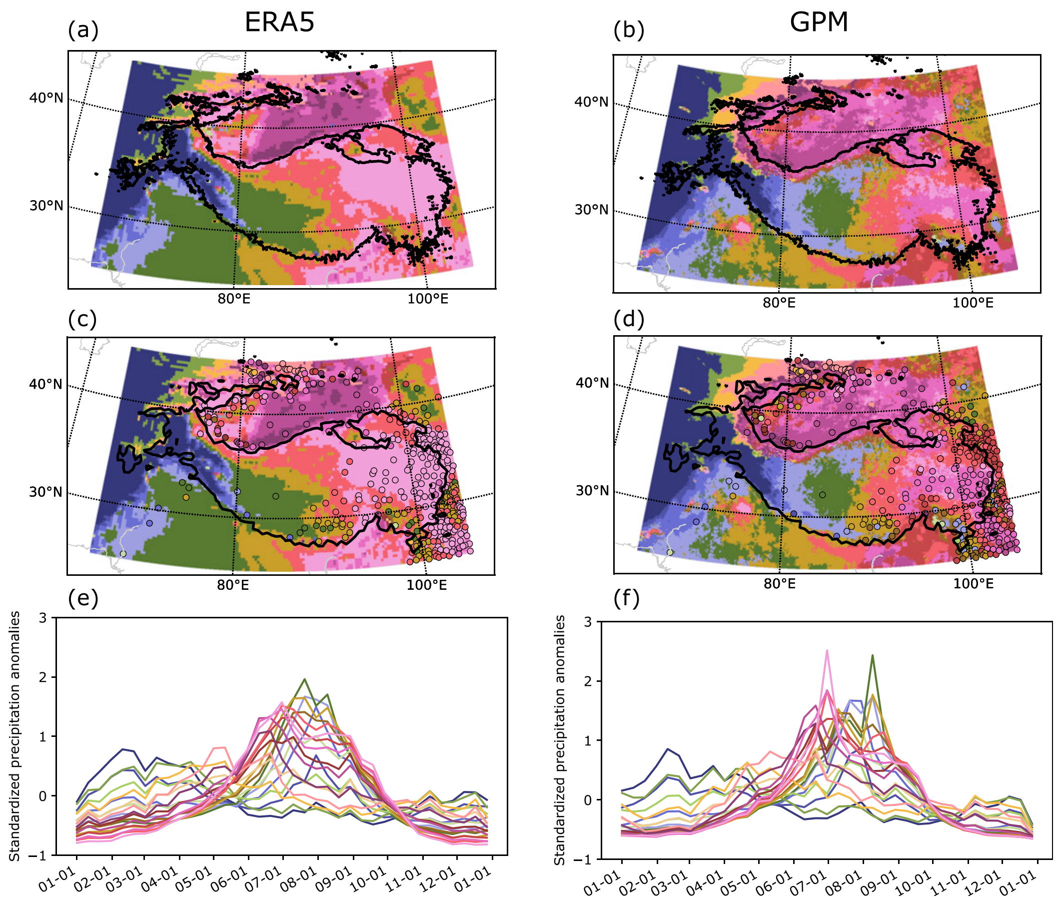

FIG. 2. The SOM classification maps of 19-yr averaged (June 2000 to May 2019) seasonal cycles of standardized precipitation for (a) ERA5 and (b) GPM. (c),(d) The same maps with classified in situ precipitation overlaid as circles. The standardized in situ observations were averaged over 18 years (June 2000 to May 2018) and classified by the SOM trained using ERA5 in (c) and GPM in (d). The black contours denote the elevation at 3000 m. Also shown are the 19-yr averaged standardized precipitation anomalies from the 20 cluster nodes for (e) ERA5 and (f) GPM.

(for in situ observations the analysis was performed to May 2018). Figure 4 shows the frequency of occurrence of each precipitation regime for all grid points. For the past 19 years, the winter peak regime in the western plateau has been robust, with dominant winter and early spring precipitation. The boundary of the winter peak has not shifted much over this 19-yr period, which shows that the region experiencing winter/early spring precipitation is relatively stationary in space and time (Figs. 4a,b). The southwestern plateau consistently experienced a late summer peak precipitation regime over the past 19 years. Some years this late summer peak regime extended mainly to northern India and the central TP (Figs. 4d,e). The early summer peak regime is predominantly found in the eastern TP and occasionally extended to the northeastern and northern plateau (Figs. 4g,h). These results indicate that the locations with higher frequencies of occurrences may be more consistently affected by the same large-scale systems, while the locations with lower frequencies of occurrences could be more sensitive to interannual variations in large-scale flows and/or to small-scale controls that are not considered here.

The classified precipitation regimes using in situ observations generally agree with those from ERA5 at the eastern plateau in terms of the spatial distribution and magnitude of the frequency of occurrence (Figs. 4f,i). Most of the in situ observations are located in the eastern plateau with an early summer peak in precipitation. The in situ data were scarce or almost nonexistent in the southwestern and western TP, which makes it difficult to examine the classification results in the winter and late summer peak regimes. Studies using in situ observations are therefore likely to fail to capture the precipitation characteristics of the winter and late summer peak regimes. Our classification suggests possible precipitation regimes and highlights the need for establishing ground-based stations in the western and southern TP.

Figures 4j and 4k show the areas and boundaries of clusters with a frequency of occurrences larger than 80% during the whole study period. The eastern, western, and southwestern plateau have robust seasonality during this period, while the seasonality at the central

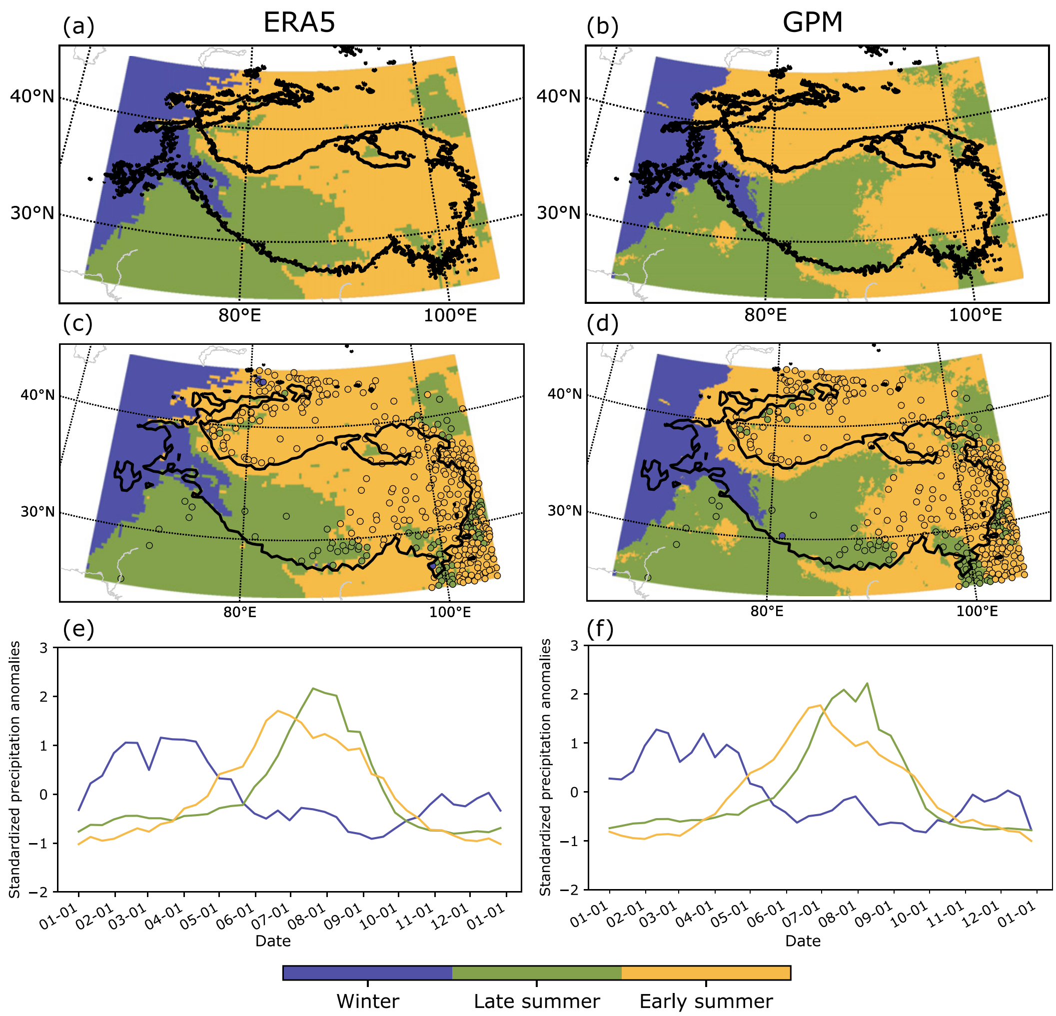

FIG. 3. As in Fig. 2, but for the regrouped classification maps (precipitation regimes) of 19-yr averaged (June 2000 to May 2019) seasonal cycles of standardized precipitation from (left) ERA5 and (right) GPM, as well as in situ observations [overlaid as circles in (c) and (d)] over 18 years (June 2000 to May 2018). (e),(f) The standardized precipitation anomalies of the spatially averaged precipitation for each precipitation regime.

and northern plateau varied from year to year. Classified in situ observations also show a robust seasonality in precipitation in the eastern and southeastern TP (Fig. 4l). The gray areas in Figs. 4j and 4k indicate transition zones where the seasonality of precipitation tended to shift on the interannual time scale. These transition zones are likely to be more sensitive to variations and changes in large-scale conditions.

4. Composite analysis

Finally, we analyzed the temporal variations of precipitation in the three robust regions that experienced the same precipitation regime over 80% of the years during 2000–19 (see Figs. 4j,k) to investigate how the regional precipitation is linked to large-scale atmospheric circulations. We applied composite analysis to examine the differences in dynamical variables in rainy seasons during wet and dry years. The rainy seasons of the three regions are January to April for the western region, July to September for the southwestern region, and May to October for the eastern region. Figure 5 shows the 41-yr ERA5 detrended precipitation anomalies spatially averaged over the three robust regions within their respective defined rainy seasons. The variations in precipitation anomalies are smallest in the western plateau and largest in the southwestern plateau. There is a significant positive trend in seasonal precipitation in the southwestern region (9 mm month^{-1} decade^{-1}), while in the western and eastern regions the trends are not significant at the 95% confidence level (not shown).

a. The western region

The western region is characterized by winter and earlier spring precipitation. During the winter, the climatological mean GPH300 maximum was located over the western Pacific

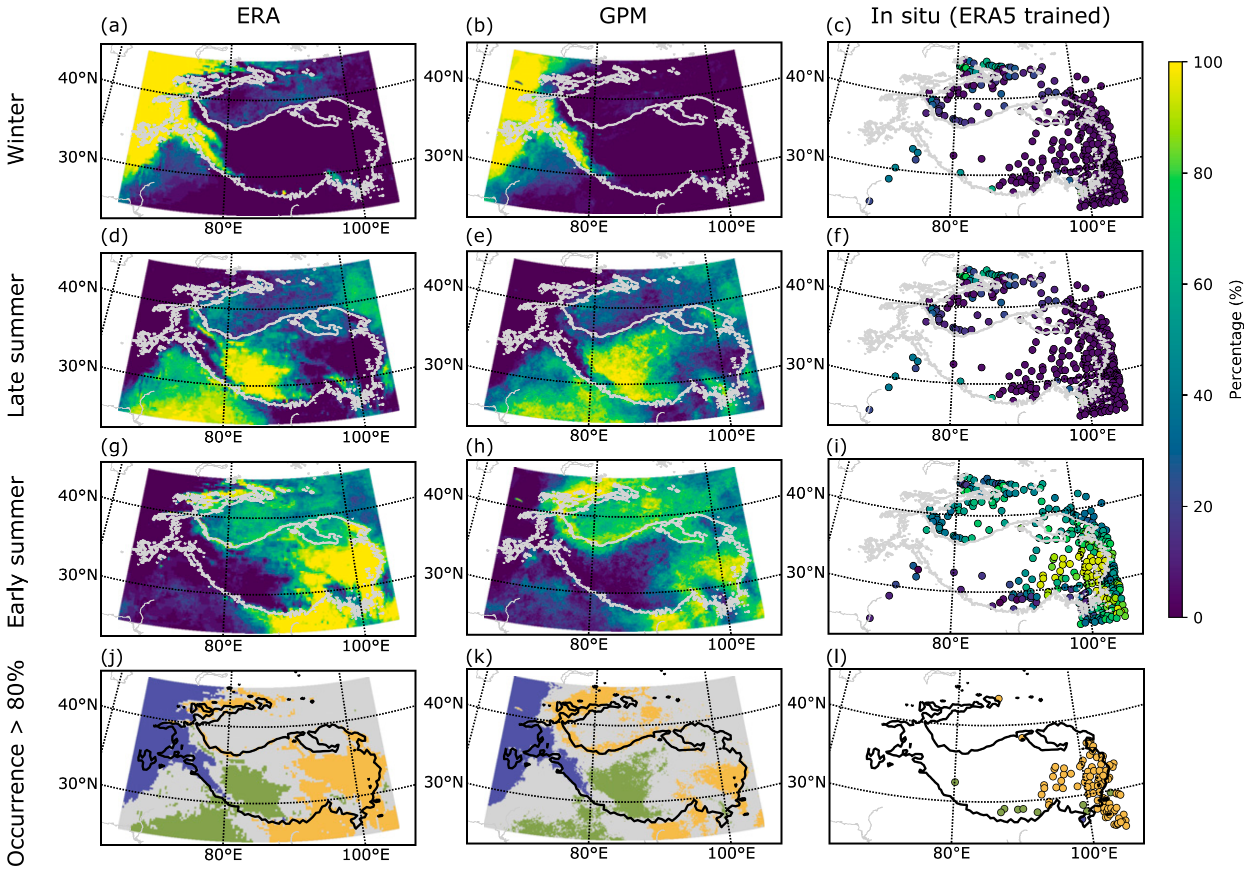

FIG. 4. Frequency of occurrences of precipitation regimes during June 2000 to May 2019 from (left) ERA5 and (center) GPM, as well as (right) during June 2000 to May 2018 from in situ observation with ERA5-trained SOM for the (a)–(c) winter peak regime, (d)–(f) late summer peak regime, and (g)–(i) early summer peak regime. Areas with a frequency of occurrences larger than 80% are shaded by the color of the main cluster for (j) ERA5, (k) GPM, and (l) in situ observations.

and decreased northward (Fig. 6a). The composite differences of GPH300 show significant negative anomalies to the west of the plateau, and positive anomalies in northeastern Asia and in a latitudinal band between the equator and about 10°N. The 41-yr average u-wind maximum at 300 hPa is between 20° and 40°N (Fig. 6b). The wet-minus-dry composite difference of u wind at 300 hPa shows significant negative anomalies over the southeastern plateau, and positive anomalies to the north, west, and south of the TP (Fig. 6b). The composite difference suggests that stronger precipitation in the western region was associated with a stronger northern flank of the subtropical westerlies to the west of the plateau near 60°E. The results are similar to those discovered by Schiemann et al. (2009) and Curio and Scherer (2016). Schiemann et al. (2009) suggested that precipitation patterns in the western TP and to the north of the plateau could be attributed to both the location of the subtropical jet and the seasonal cycles of the jet. In previous studies, the winter precipitation in the western and southwestern TP was found to be orographically forced during intense westerly disturbances (Cannon et al. 2016; Hunt et al. 2018). Our results confirm that precipitation anomalies in this region are associated with the changes in the location of westerlies.

The wet-minus-dry composite differences in the wind components at 850 hPa show positive anomalies of westerly wind between 20°–30°N to the west of the TP (Fig. 6c) and southerly wind to the west of the TP (Fig. 6d). In addition, the composite differences in vertically integrated moisture fluxes show that increased precipitation in the western TP was significantly correlated with increased moisture transport from the west of the plateau (Fig. 6e). The results indicate that the positive anomalies of westerlies, which are the prevailing winds during this season, together with the stronger positive anomalies of southerly wind are most likely responsible for bringing moist air for the precipitation, which is consistent with the findings of Dai and Wang (2017). Our results also agree with Kar and Rana (2014), who found a strong correlation between precipitation over northwest India and zonal and meridional wind over the Arabian Sea. Overall, precipitation variations in the western TP are strongly linked to synoptic-scale variations in the westerly and southerly winds to the west/southwest of the TP, and moisture transported from the west of the TP.

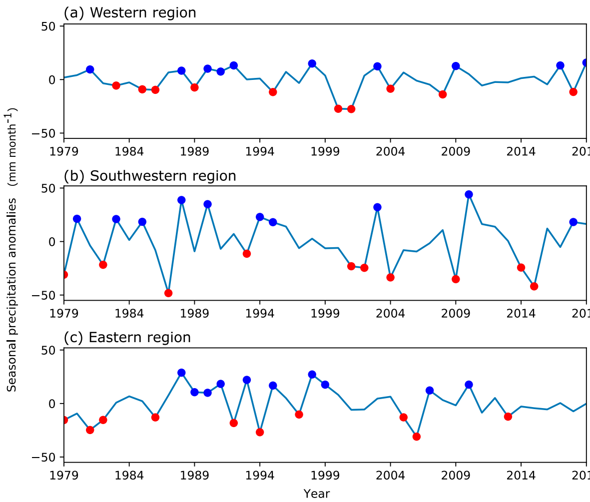

FIG. 5. Time series of detrended seasonal precipitation anomalies from 1979 to 2019 in the (a) western region, (b) southwestern region, and (c) eastern region. The blue dots denote the wet years with 10 highest anomalies and the red dots the dry years with 10 lowest anomalies.

b. The southwestern region

During the rainy season of the southwestern region, the 41-yr average GPH300 in the domain is highest between 15° and 35°N (Fig. 7a), which can be attributed to the South Asian high (Flohn 1957; Mason and Anderson 1963). Previous studies have shown that the formation of the South Asian high is associated with strong summertime land surface heating and latent heat release, which can alter precipitation caused by the Asian summer monsoon (Zhou et al. 2020). The relatively strong northward gradient in GPH300 (Fig. 7a) in the northern portion of the South Asian high results in a band of high climatological mean u wind between roughly 30° and 50°N (Fig. 7b). During the wet (dry) southwestern TP years, the composite anomalies of GPH300 are significantly positive (negative) around 30°–40°N (i.e., stronger precipitation in the southwest TP was associated with positive GPH300 anomalies over the plateau). This change in GPH300 most likely caused the westerlies to strengthen to the northwest of the TP and weaken in the southwestern plateau during wet years, and vice versa during dry years. Stronger westerlies at 300 hPa over the southwestern region could reduce the regional precipitation by suppressing the development of convection due to increased vertical wind shear (e.g., Mölg et al. 2014). Thus, our results show that the precipitation over the southwestern TP is closely linked to changes in the strength of the South Asian high and upper-tropospheric westerly winds over the southwestern plateau.

During wet years in the southwestern region, the average MSLP was lower over northern India, Pakistan, and Saudi Arabia and higher over the northwestern Pacific Ocean compared to dry years (Fig. 7c). Anticyclonic circulations can be found in the climatological mean u and v winds at 850 hPa centered over the Arabian Sea with a cross-equatorial Somali jet and cyclonic circulation over the northern Bay of Bengal (Figs. 7d,e), which are typical circulation patterns during the South Asian summer monsoon seasons (Ju and Slingo 1995; Ye and Wu 1998; Ding and Sikka 2006). These circulation systems became significantly stronger during wet southwestern TP years, when the MSLP exhibits negative anomalies, while during dry years the circulations became weaker and the MSLP anomalies were positive. The u and v components of the winds also show that positive (negative) anomalies of low-level westerly and southerly winds were found over the Arabian Sea during the wet (dry) years.

The stronger low-level westerly winds together with southerly wind led to stronger moisture transport toward the southwestern TP over the Arabian Sea (Fig. 7f). Therefore, the precipitation in the southwestern region was likely affected by the low pressure system over Pakistan and Saudi Arabia, and the low-level jet in the southwestern part of the domain. Li and Wang (2005) showed that a strong WNPSM is associated with increased rainfall over the eastern TP and suppressed rainfall in the southwestern TP. Our results reveal that the WNPSM associated with low-latitude westerly winds over the western Pacific and the South China Sea was not significantly stronger or weaker during the wet southwestern TP years. Therefore, it is hard to tell how much the WNPSM impacted regional precipitation in the southwestern TP. Overall, precipitation changes over the southwestern TP were related to changes in ISM flows, the South Asian high, and upper-tropospheric winds.

c. The eastern region

The rainy season of the eastern region is defined as May–October, during which the region can be affected by several circulation systems with different spatiotemporal distributions. The 41-yr average MSLP during this season is very similar to the climatological MSLP during the rainy season of the southwestern region, with lower values over northern India and Saudi Arabia and higher values over the western North Pacific (Fig. 8c). The MSLP over the western North Pacific has previously been used as an indicator for the strength of the EASM (e.g., Shi and Zhu 1996), which is strongly correlated with the western North Pacific subtropical high (Lee et al. 2013). The MSLP over the western North Pacific was higher (lower) during the wet (dry) years in the eastern region, while in the Arabian Sea the MSLP was lower (higher) during the wet (dry) years, which indicates that precipitation changes in the eastern TP were related to changes in the strength of the high pressure and low pressure systems in these two areas. During the wet years in the eastern region, the 850-hPa easterly wind was anomalously strong over the western North Pacific, concurrent with weaker westerly winds over the South China Sea and stronger westerly winds to the south of India (Fig. 8d). At the same time the southerly winds were anomalously strong over the western North Pacific and the Bay of Bengal (Fig. 8e). The anomalously strong westerly and easterly winds as well as southerly winds indicate that a stronger subtropical anticyclonic circulation and Somali jet can potentially bring more moisture into the eastern TP, which leads to stronger precipitation in this region. Our results are consistent with previous

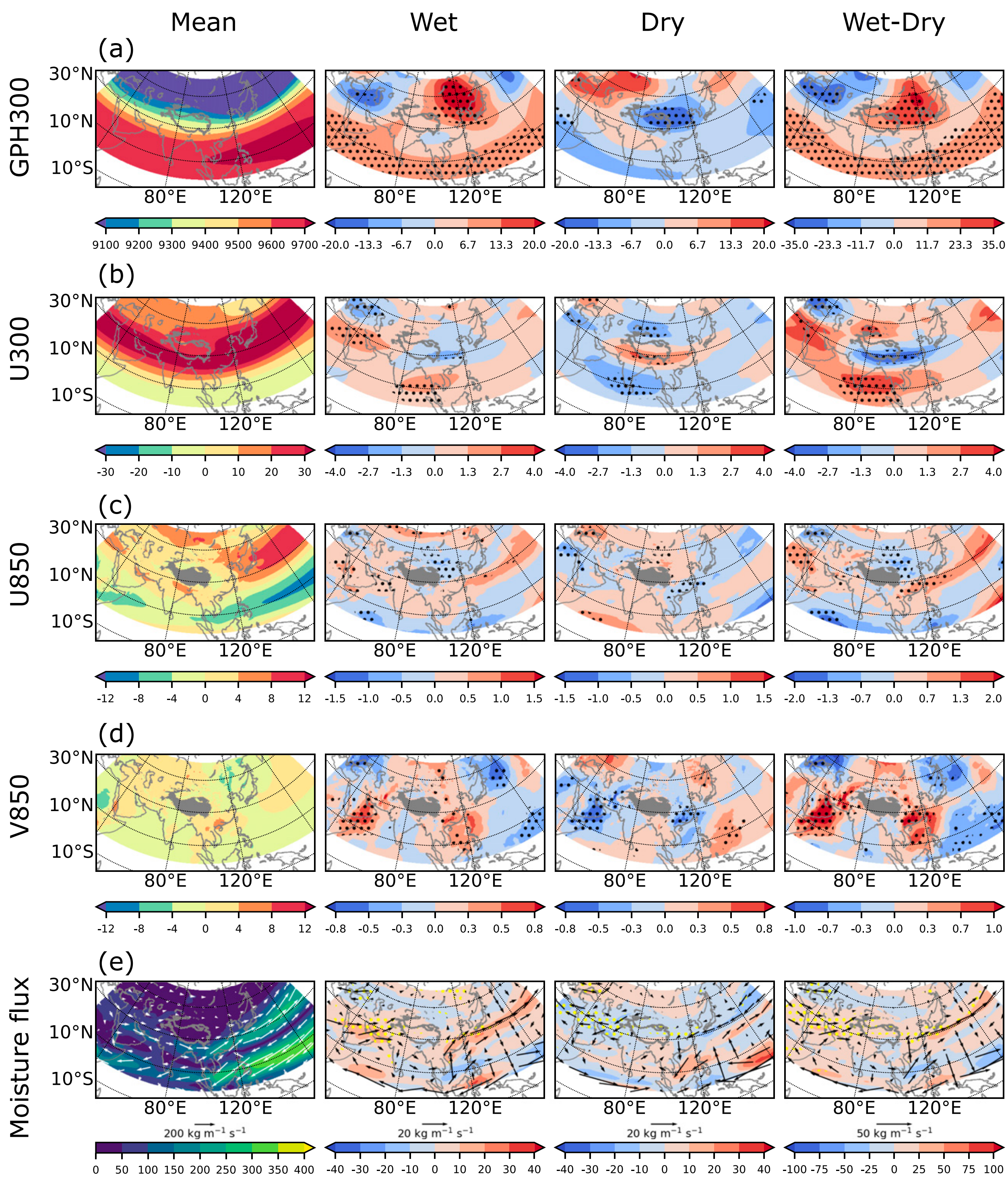

FIG. 6. For the western region during January–April, the (left) 41-yr average, (center left) composite wet-year minus the climatological average not including the wet years, (center right) composite dry-year minus the climatological average not including the dry years, and (right) composite wet-year minus dry-year differences of (a) 300-hPa geopotential height (gpm), (b) 300-hPa u wind (m s^{-1}), (c) 850-hPa u wind (m s^{-1}), (d) 850-hPa v wind (m s^{-1}), and (e) vertically integrated moisture flux (kg m^{-1} s^{-1}) from ERA5 during the rainy season from 1979 to 2019. The arrows in the last three columns in (e) show the change in direction of the moisture fluxes, and the shading shows the difference in the total magnitude of the moisture fluxes. Black dots in (a)–(d) and yellow dots in (e) represent differences significant at the 95% confidence level according to a Student's t test.

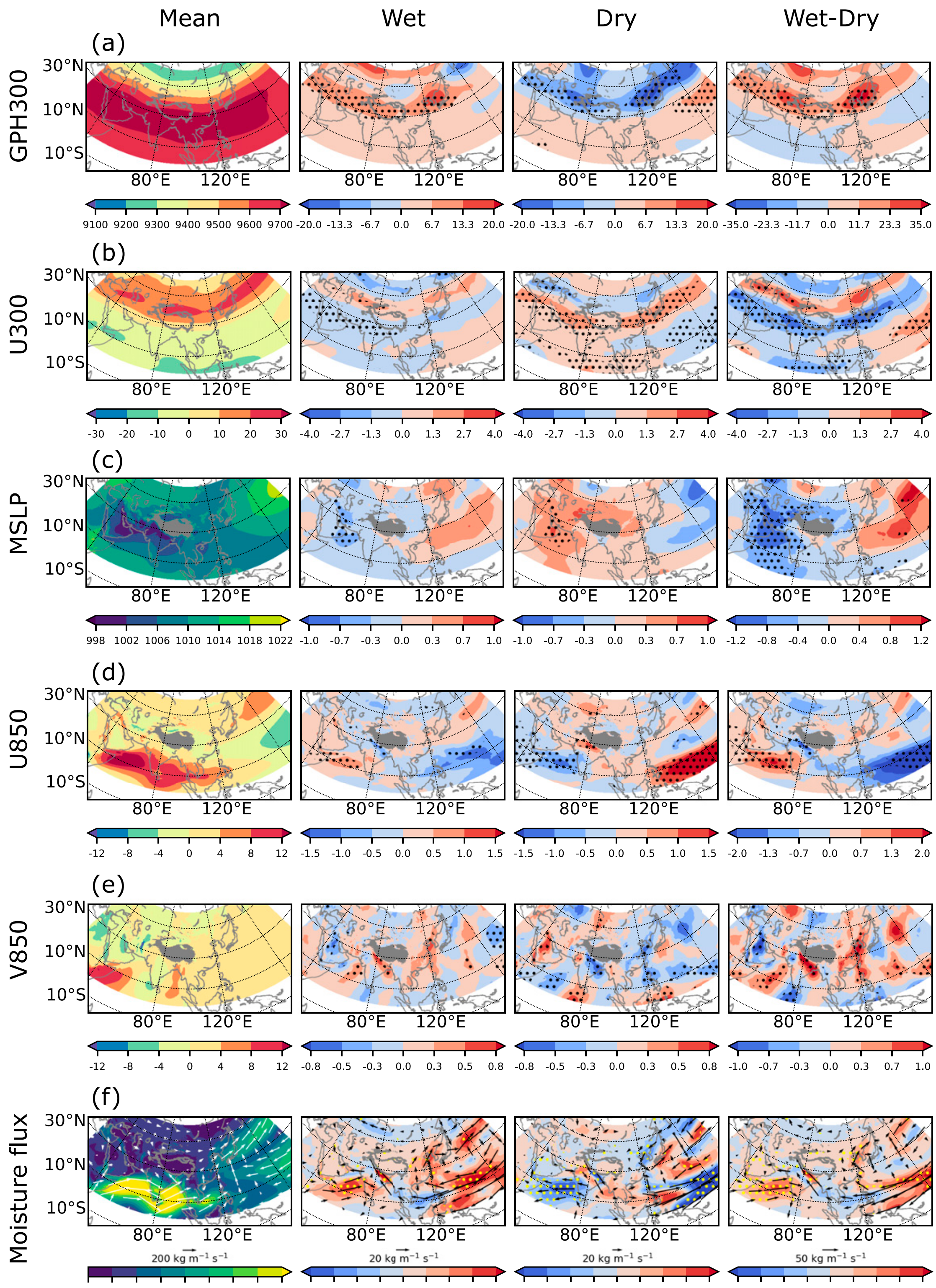

FIG. 7. As in Fig. 6, but for the southwestern region during July–September for (a) 300-hPa geopotential height (gpm), (b) 300-hPa u wind (m s^{-1}), (c) mean sea level pressure (hPa), (d) 850-hPa u wind (m s^{-1}), (e) 850-hPa v wind (m s^{-1}), and (f) vertically integrated moisture flux (kg m^{-1} s^{-1}).

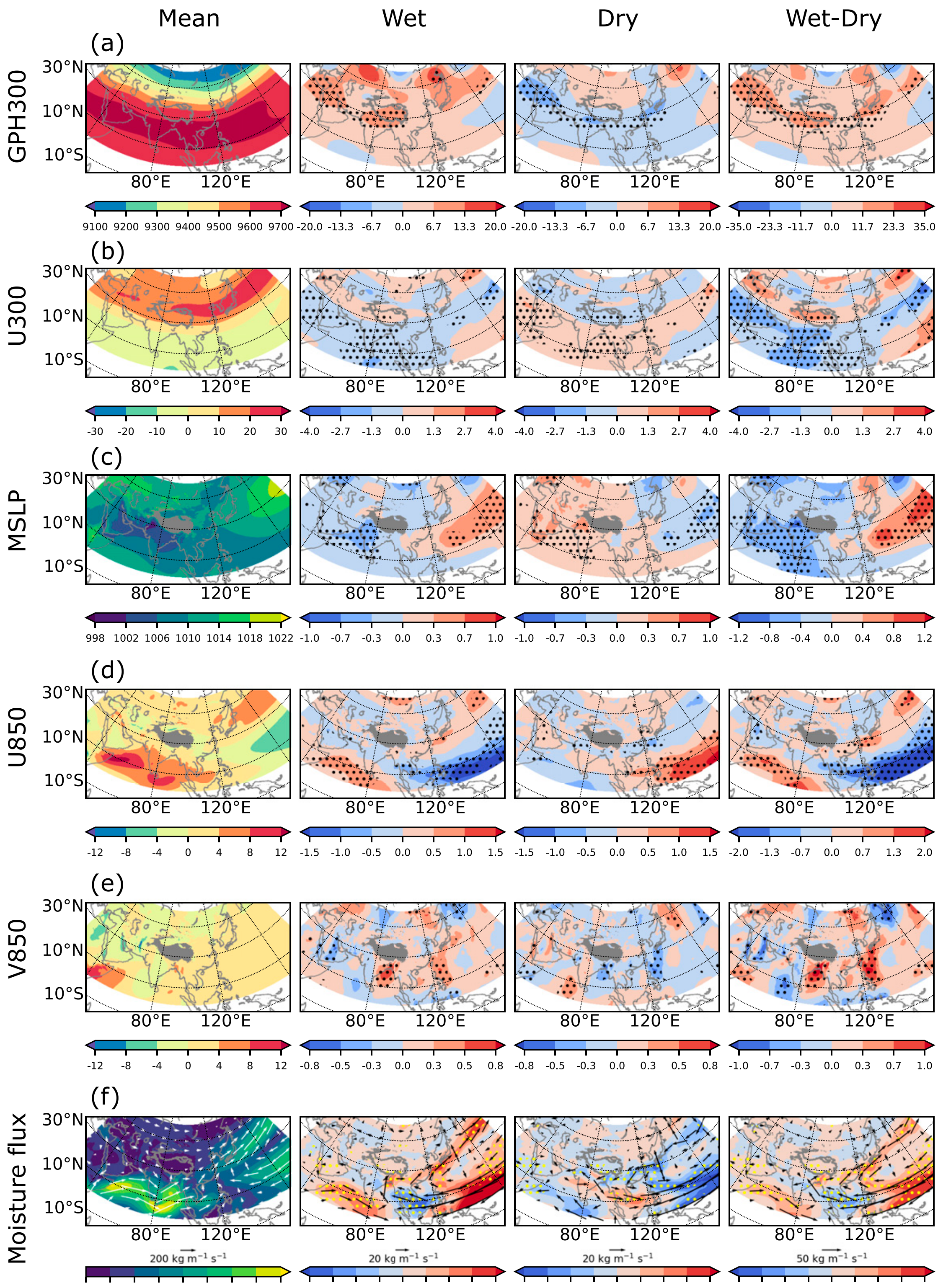

FIG. 8. As in Fig. 7, but for the eastern region during May–October.

studies that have shown that in a strong EASM year, more moisture is transported to central-eastern China (Zhang et al. 2016) and eastern TP (Bothe et al. 2010), resulting in increased summer precipitation around these regions.

Similar to the southwestern region, the South Asian high is evident in the 41-yr averaged GPH300 as the higher GPH300 values between 10° and 30°N during the rainy season of the eastern region (Fig. 8a). The wet-minus-dry composite difference in GPH300 is significantly positive to the south of the TP. The anomalous high could be induced by stronger precipitation in the eastern TP due to stronger condensational heating (Zhang et al. 2016). The diabatic condensational heating could have led to a stronger vertical upward motion in the eastern TP and stronger subsidence to the west of the TP. Our results show a similar pattern to the one in Zhang et al. (2016), with GPH300 anomalies located in the southwestern plateau associated with precipitation changes in the eastern region. On the contrary, the anomalous westerlies at 300 hPa (Fig. 8b) are weaker than those associated with the southwestern region (Fig. 7b), which suggests that the suppression of convection by vertical wind shear plays a less important role for precipitation changes in the eastern TP.

In general, the wet years in the eastern region were related to a stronger high pressure system over the western North Pacific associated with the EASM. Figure 8f shows that during the wet years, there was an anomalously stronger moisture flux to the southeast of the plateau associated with the ISM flowing to the southeastern plateau. Additionally, there were anomalous southeasterly moisture fluxes from the western flank of the EASM circulation extending from the South China Sea to the southeast of the TP where the southerly wind anomalies were strong (Fig. 8e). These two flows may converge at the southeastern TP; however, it is difficult to conclude whether the EASM contributes to the anomalously strong moisture flux at the southeastern TP. Curio et al. (2015) showed that the moisture contribution from the EASM to precipitation in the eastern TP was insignificant during their 12-yr study period, while Zhang (2019) and Du et al. (2020) found that precipitation fluctuations to the northeast of the TP could be related to the EASM and ISM. Future studies on moisture tracing could be helpful to clarify the contributions from the EASM to the precipitation over the TP.

The main difference between the atmospheric circulations associated with precipitation in the southwestern and eastern regions is that wet years in the southwestern region were mainly associated with increased moisture transport toward the TP over the Arabian Sea, while wet years in the eastern region were associated with significant moisture flux anomalies over the southern Arabian Sea, which extended to the Bay of Bengal, and over the South China Sea. We note that the moisture flux composites for the southwestern region also show some significant differences over the Pacific, but it is not clear whether these moisture fluxes affect the precipitation in the southwestern TP; the significant correlations may be coincidental due to covarying systems. Previous studies have suggested that the EASM interacts frequently with the ISM and that it is hard to separate the contribution from each system (Wu 2017). Our study shows no significant impacts from the EASM on the interannual precipitation variations in the southwestern region. Hence, the wet and dry years in the eastern TP were more closely related to variations in the ISM and the anticyclonic circulation over the western North Pacific associated with the EASM, while the wet and dry years in the southwestern TP were related to the ISM.

5. Conclusions and discussion

This study used precipitation data over the TP from satellite, reanalysis, and in situ observations to classify the TP into regions according to the seasonal cycles of precipitation using the objective SOM method. From the classification results, three precipitation regimes with distinct seasonality in precipitation were found, centered at the western, southwestern, and eastern plateau. While the spatial distribution of the three regimes is similar to what previous studies have found, the longer and well-sampled data over the study region provide much more accurate boundaries of the regimes. We also presented the robustness and variations of the precipitation regimes on an interannual time scale, as well as the large-scale atmosphere systems associated with the year-to-year variations in precipitation in three regions with robust precipitation regimes.

Precipitation over the western TP mainly occurred in winter and earlier spring. This winter peak precipitation regime was the most robust regime and has not changed much in spatial extent during the past 19 years. The composite analysis indicates that interannual precipitation variations in this region were strongly related to the strength of westerlies at the northern flank of the climatological midlatitude westerly jet.

The precipitation variations in the southwestern and eastern regions were both related to variations in the South and East Asian summer monsoons but through different mechanisms. The late summer peak precipitation regime in the southwestern region exhibited dominantly summer precipitation from July to September. This regime was robust in the southwestern region and northern India, and often also appeared in central TP. Increases in precipitation and moisture transport in the southwestern region were associated with an anomalously strong South Asian high and ISM.

The eastern region was characterized by a rainy season from May to October, which is referred to as the early summer peak precipitation regime. This regime was robust in the eastern TP and occasionally extended to the central and northern TP and to the north of the TP. The precipitation in the eastern TP was correlated with variations in the ISM and the anticyclonic circulation over the western North Pacific. Another significant feature during the wet years in the eastern region was a stronger South Asian high to the southwest of the TP, likely due to increased latent heating generated by the precipitation.

There are a few caveats worth mentioning here. The most important issue is the data used, which has a direct effect on the classification results. It is well known that the satellite-based and ERA5 precipitation estimates have some uncertainty for snow and frozen hydrometeors in mountainous regions. Previous studies have suggested that ERA5 overestimates snow precipitation, which leads to a cold bias over the TP (e.g., Orsolini et al. 2019; Wang et al. 2020). This is especially true for the Himalayas, northwestern TP, and eastern TP during the cold season. Moreover, because of the sparsity of gauge stations in a large portion of the TP and surrounding regions, biases in precipitation estimates from remote sensors can only partly be corrected through gauge calibrations. With that said, compared to older spaceborne radars, the Dual-Frequency Precipitation Radar of GPM has a higher sensitivity for solid and light precipitation (Casella et al. 2017; Tang et al. 2017) and it has been repeatedly shown that GPM exhibits improved capabilities for snowfall detection both over the TP (Ma et al. 2016) and in other mountain regions (Wen et al. 2016). It is possible that these uncertainties in snow precipitation could influence our results, especially in the western plateau where winter precipitation dominates. However, given that this region shows the most distinct seasonality out of the three precipitation regimes we identified and there is a high agreement between ERA5 and GPM, it is unlikely that the overall conclusions in this region are affected. The largest mismatches between ERA5 and GPM are found in north-central TP where the GPM-derived classification finds a larger frequency of occurrence of the late summer peak precipitation regime compared with ERA5. Reliable long-term in situ observations, particularly in the central and western plateau, would be extremely helpful to reduce the uncertainty in the analyses in general, and to resolve the disparity between the GPM data and ERA5 in particular.

Seasonal precipitation over the TP results from interactions among different large-scale atmospheric systems. We identified the boundaries of three different precipitation regimes and show that the transition zones are located at the central and northern TP. These transition zones are likely to have varying seasonal cycles of precipitation on an interannual time scale, which could be related to interannual changes in the large-scale circulation and/or more local processes. In this study we have focused on the interannual precipitation variations in three regions with robust precipitation regimes. We have also tried different thresholds to merge the original 20 clusters into varying numbers of larger groups. However, we found that the additional groups exhibited similar features to the three leading precipitation regimes used in this study, and that the extraneous regimes were not robust on an interannual time scale. We therefore decided to keep the three leading precipitation regimes. We have also performed an initial analysis on the link between the seasonal precipitation amounts and interannual variabilities of different monsoon indices (e.g., from Wang et al. 2008) and subtropical high indices, but we did not find any statistically significant relationships, likely because precipitation is a nonlinear process that results from interactions between large-scale circulations and local processes. For example, surface radiative heating is one of the important factors that lead to intensive convective precipitation over the plateau (Li et al. 2008). This study did not explicitly consider such local factors, nor did it explicitly consider precipitation variations with elevation, which have been shown to be important over the TP in a previous study (Sun et al. 2020). A moisture budget analysis, as performed by, for example, Zhu et al. (2020) over the south-central TP, could be applied to the entire TP in future studies to understand the contributions from dynamic and thermodynamic components to regional precipitation. Nevertheless, the results from this study provide a foundation for understanding the regional precipitation characteristics over the TP, upon which future studies can build to further investigate mechanisms for precipitation formation at different spatial scales over the TP.

Acknowledgments. We thank three anonymous reviewers for their constructive comments and suggestions. This work was supported by the Strategic Priority Research Program of Chinese Academy of Sciences (Grant XDA20060401), the Swedish National Space Agency (SNSA: 188/18), and the Swedish Foundation for International Cooperation in Research and Higher Education (CH2019-8377). It is a contribution to the Swedish national strategic research programs BECC and MERGE. The ERA5 data were generated using Copernicus Climate Change Service Information (https://www.ecmwf.int/en/forecasts/datasets/reanalysis-datasets/era5). The GPM product was provided by NASA (https://gpm.nasa.gov/data-access/downloads/gpm), and in situ observations were obtained from the China Meteorological Administration (CMA) and NOAA Global Historical Climatology Network (GHCN; https://www.ncdc.noaa.gov/ghcn-daily-description). The self-organizing map (SOM) toolbox (version 2.0) can be found at the website of the Laboratory of Computer and Information Science at the Helsinki University of Technology (http://www.cis.hut.fi/somtoolbox/).

REFERENCES

Bibi, S., L. Wang, X. Li, J. Zhou, D. Chen, and T. Yao, 2018: Climatic and associated cryospheric, biospheric, and hydrological changes on the Tibetan Plateau: A review. *Int. J. Climatol.*, **38**, e1–e17, https://doi.org/10.1002/joc.5411.

Bothe, O., K. Fraedrich, and X. Zhu, 2010: The large-scale circulations and summer drought and wetness on the Tibetan Plateau. *Int. J. Climatol.*, **30**, 844–855, https://doi.org/10.1002/joc.1946.

Cannon, F., L. M. V. Carvalho, C. Jones, and J. Norris, 2016: Winter westerly disturbance dynamics and precipitation in the western Himalaya and Karakoram: A wave-tracking approach. *Theor. Appl. Climatol.*, **125**, 27–44, https://doi.org/10.1007/s00704-015-1489-8.

Casella, D., G. Panegrossi, P. Sanò, A. C. Marra, S. Dietrich, B. T. Johnson, and M. S. Kulie, 2017: Evaluation of the GPM-DPR snowfall detection capability: Comparison with CloudSat-CPR. *Atmos. Res.*, **197**, 64–75, https://doi.org/10.1016/j.atmosres.2017.06.018.

Chang, C.-P., Y. Zhang, and T. Li, 2000: Interannual and interdecadal variations of the East Asian summer monsoon and tropical Pacific SSTs. Part I: Roles of the subtropical ridge. *J. Climate*, **13**, 4310–4325, https://doi.org/10.1175/1520-0442(2000)013<4310:IAIVOT>2.0.CO;2.

Chen, D., and H. W. Chen, 2013: Using the Köppen classification to quantify climate variation and change: An example for 1901–2010. *Environ. Dev.*, **6**, 69–79, https://doi.org/10.1016/j.envdev.2013.03.007.

——, and Coauthors, 2015: Assessment of past, present and future environmental changes on the Tibetan Plateau. *Chin. Sci. Bull.*, **60**, 3025–3035, https://doi.org/10.1360/N972014-01370.

Curio, J., and D. Scherer, 2016: Seasonality and spatial variability of dynamic precipitation controls on the Tibetan Plateau. *Earth Syst. Dyn.*, **7**, 767–782, https://doi.org/10.5194/esd-7-767-2016.

——, F. Maussion, and D. Scherer, 2015: A 12-year high-resolution climatology of atmospheric water transport over the Tibetan Plateau. *Earth Syst. Dyn.*, **6**, 109–124, https://doi.org/10.5194/esd-6-109-2015.

Dai, X.-G., and P. Wang, 2017: A new classification of large-scale climate regimes around the Tibetan Plateau based on seasonal circulation patterns. *Adv. Climate Change Res.*, **8**, 26–36, https://doi.org/10.1016/j.accre.2017.01.001.

Ding, Y., and J. C. L. Chan, 2005: The East Asian summer monsoon: An overview. *Meteor. Atmos. Phys.*, **89**, 117–142, https://doi.org/10.1007/s00703-005-0125-z.

——, and D. R. Sikka, 2006: Synoptic systems and weather. *The Asian Monsoon*, Springer, 131–201.

Du, W., S. Kang, X. Qin, Z. Ji, W. Sun, J. Chen, J. Yang, and D. Chen, 2020: Can summer monsoon moisture invade the Jade Pass in northwestern China? *Climate Dyn.*, **55**, 3101–3115, https://doi.org/10.1007/s00382-020-05423-y.

Feng, L., and T. Zhou, 2012: Water vapor transport for summer precipitation over the Tibetan Plateau: Multidata set analysis. *J. Geophys. Res.*, **117**, D20114, https://doi.org/10.1029/2011JD017012.

Flohn, H., 1957: Large-scale aspects of the "summer monsoon" in South and East Asia. *J. Meteor. Soc. Japan*, **35A**, 180–186, https://doi.org/10.2151/jmsj1923.35A.0_180.

Ge, F., F. Sielmann, X. Zhu, K. Fraedrich, X. Zhi, T. Peng, and L. Wang, 2017: The link between Tibetan Plateau monsoon and Indian summer precipitation: A linear diagnostic perspective. *Climate Dyn.*, **49**, 4201–4215, https://doi.org/10.1007/s00382-017-3585-1.

Hersbach, H., and Coauthors, 2018: Operational global reanalysis: Progress, future directions and synergies with NWP. ECMWF ERA Rep. Series 27, 63 pp., https://doi.org/10.21957/tkic6g3wm.

Hou, A. Y., and Coauthors, 2014: The Global Precipitation Measurement Mission. *Bull. Amer. Meteor. Soc.*, **95**, 701–722, https://doi.org/10.1175/BAMS-D-13-00164.1.

Huang, Y., B. Wang, X. Li, and H. Wang, 2018: Changes in the influence of the western Pacific subtropical high on Asian summer monsoon rainfall in the late 1990s. *Climate Dyn.*, **51**, 443–455, https://doi.org/10.1007/s00382-017-3933-1.

Hunt, K. M. R., J. Curio, A. G. Turner, and R. Schiemann, 2018: Subtropical westerly jet influence on occurrence of western disturbances and Tibetan Plateau vortices. *Geophys. Res. Lett.*, **45**, 8629–8636, https://doi.org/10.1029/2018GL077734.

Immerzeel, W. W., and Coauthors, 2020: Importance and vulnerability of the world's water towers. *Nature*, **577**, 364–369, https://doi.org/10.1038/s41586-019-1822-y.

Ju, J., and J. Slingo, 1995: The Asian summer monsoon and ENSO. *Quart. J. Roy. Meteor. Soc.*, **121**, 1133–1168, https://doi.org/10.1002/qj.49712152509.

Kar, S. C., and S. Rana, 2014: Interannual variability of winter precipitation over northwest India and adjoining region: Impact of global forcings. *Theor. Appl. Climatol.*, **116**, 609–623, https://doi.org/10.1007/s00704-013-0968-z.

Kohonen, T., 1982: Self-organized formation of topologically correct feature maps. *Biol. Cybern.*, **43**, 59–69, https://doi.org/10.1007/BF00337288.

Kukulies, J., D. Chen, and M. Wang, 2019: Temporal and spatial variations of convection and precipitation over the Tibetan Plateau based on recent satellite observations. Part I: Cloud climatology derived from *CloudSat* and *CALIPSO*. *Int. J. Climatol.*, **39**, 5396–5412, https://doi.org/10.1002/joc.6162.

——, ——, and ——, 2020: Temporal and spatial variations of convection, clouds and precipitation over the Tibetan Plateau from recent satellite observations. Part II: Precipitation climatology derived from Global Precipitation Measurement Mission. *Int. J. Climatol.*, **40**, 4858–4875, https://doi.org/10.1002/joc.6493.

Lau, K.-M., K.-M. Kim, and S. Yang, 2000: Dynamical and boundary forcing characteristics of regional components of the Asian summer monsoon. *J. Climate*, **13**, 2461–2482, https://doi.org/10.1175/1520-0442(2000)013<2461:DABFCO>2.0.CO;2.

Lee, S.-S., Y.-W. Seo, K.-J. Ha, and J.-G. Jhun, 2013: Impact of the western North Pacific subtropical high on the East Asian monsoon precipitation and the Indian Ocean precipitation in the boreal summertime. *Asia-Pacific J. Atmos. Sci.*, **49**, 171–182, https://doi.org/10.1007/s13143-013-0018-x.

Li, T., and B. Wang, 2005: A review on the western North Pacific monsoon: Synoptic-to-interannual variabilities. *Terr. Atmos. Oceanic Sci.*, **16**, 285, https://doi.org/10.3319/TAO.2005.16.2.285(A).

Li, Y., Y. Wang, Y. Song, L. Hu, S. Gao, and R. Fu, 2008: Characteristics of summer convective systems initiated over the Tibetan Plateau. Part I: Origin, track, development, and precipitation. *J. Appl. Meteor. Climatol.*, **47**, 2679–2695, https://doi.org/10.1175/2008JAMC1695.1.

Liu, X., and B. Chen, 2000: Climatic warming in the Tibetan Plateau during recent decades. *Int. J. Climatol.*, **20**, 1729–1742, https://doi.org/10.1002/1097-0088(20001130)20:14<1729::AID-JOC556>3.0.CO;2-Y.

——, Z. Cheng, L. Yan, and Z.-Y. Yin, 2009: Elevation dependency of recent and future minimum surface air temperature trends in the Tibetan Plateau and its surroundings. *Global Planet. Change*, **68**, 164–174, https://doi.org/10.1016/j.gloplacha.2009.03.017.

Ma, Y., G. Tang, D. Long, B. Yong, L. Zhong, W. Wan, and Y. Hong, 2016: Similarity and error intercomparison of the GPM and its predecessor—TRMM Multisatellite Precipitation Analysis using the best available hourly gauge network over the Tibetan Plateau. *Remote Sens.*, **8**, 569, https://doi.org/10.3390/rs8070569.

Mason, R. B., and C. E. Anderson, 1963: The development and decay of the 100-mb summertime anticyclone over southern Asia. *Mon. Wea. Rev.*, **91**, 3–12, https://doi.org/10.1175/1520-0493(1963)091<0003:TDADOT>2.3.CO;2.

Maussion, F., D. Scherer, T. Mölg, E. Collier, J. Curio, and R. Finkelnburg, 2014: Precipitation seasonality and variability over the Tibetan Plateau as resolved by the High Asia Reanalysis. *J. Climate*, **27**, 1910–1927, https://doi.org/10.1175/JCLI-D-13-00282.1.

Mölg, T., F. Maussion, and D. Scherer, 2014: Mid-latitude westerlies as a driver of glacier variability in monsoonal High Asia. *Nat. Climate Change*, **4**, 68–73, https://doi.org/10.1038/nclimate2055.

——, ——, E. Collier, J. C. H. Chiang, and D. Scherer, 2017: Prominent midlatitude circulation signature in High Asia's surface climate during monsoon. *J. Geophys. Res. Atmos.*, **122**, 12 702–12 712, https://doi.org/10.1002/2017JD027414.

Mwasiagi, J. I., Ed., 2011: *Self Organizing Maps—Applications and Novel Algorithm Design*. InTech, 716 pp.

Orsolini, Y., and Coauthors, 2019: Evaluation of snow depth and snow cover over the Tibetan Plateau in global reanalyses using in situ and satellite remote sensing observations. *Cryosphere*, **13**, 2221–2239, https://doi.org/10.5194/tc-13-2221-2019.

Park, H.-S., J. C. H. Chiang, and S. Bordoni, 2012: The mechanical impact of the Tibetan Plateau on the seasonal evolution of the

South Asian monsoon. *J. Climate*, **25**, 2394–2407, https://doi.org/10.1175/JCLI-D-11-00281.1.

Sato, T., 2009: Influences of subtropical jet and Tibetan Plateau on precipitation pattern in Asia: Insights from regional climate modeling. *Quat. Int.*, **194**, 148–158, https://doi.org/10.1016/j.quaint.2008.07.008.

Schiemann, R., D. Lüthi, and C. Schär, 2009: Seasonality and interannual variability of the westerly jet in the Tibetan Plateau region. *J. Climate*, **22**, 2940–2957, https://doi.org/10.1175/2008JCLI2625.1.

Shi, N., and Q. Zhu, 1996: An abrupt change in the intensity of the East Asian summer monsoon index and its relationship with temperature and precipitation over East China. *Int. J. Climatol.*, **16**, 757–764, https://doi.org/10.1002/(SICI)1097-0088(199607)16:7<757::AID-JOC50>3.0.CO;2-5.

Sun, H., F. Su, J. Huang, T. Yao, Y. Luo, and D. Chen, 2020: Contrasting precipitation gradient characteristics between westerlies and monsoon dominated upstream river basins in the Third Pole. *Chin. Sci. Bull.*, **65**, 91–104, https://doi.org/10.1360/TB-2019-0491.

Tanaka, M., 1992: Intraseasonal oscillation and the onset and retreat dates of the summer monsoon over East, Southeast Asia and the western Pacific region using GMS high cloud amount data. *J. Meteor. Soc. Japan*, **70**, 613–629, https://doi.org/10.2151/jmsj1965.70.1B_613.

Tang, G., Y. Wen, J. Gao, D. Long, Y. Ma, W. Wan, and Y. Hong, 2017: Similarities and differences between three coexisting spaceborne radars in global rainfall and snowfall estimation. *Water Resour. Res.*, **53**, 3835–3853, https://doi.org/10.1002/2016WR019961.

Thorndike, R. L., 1953: Who belongs in the family? *Psychometrika*, **18**, 267–276, https://doi.org/10.1007/BF02289263.

Wang, B., and LinHo, 2002: Rainy season of the Asian–Pacific summer monsoon. *J. Climate*, **15**, 386–398, https://doi.org/10.1175/1520-0442(2002)015<0386:RSOTAP>2.0.CO;2.

——, R. Wu, and K.-M. Lau, 2001: Interannual variability of the Asian summer monsoon: Contrasts between the Indian and the western North Pacific–East Asian monsoons. *J. Climate*, **14**, 4073–4090, https://doi.org/10.1175/1520-0442(2001)014<4073:IVOTAS>2.0.CO;2.

——, Z. Wu, J. Li, J. Liu, C. P. Chang, Y. Ding, and G. Wu, 2008: How to measure the strength of the East Asian summer monsoon. *J. Climate*, **21**, 4449–4463, https://doi.org/10.1175/2008JCLI2183.1.

Wang, X., V. Tolksdorf, M. Otto, and D. Scherer, 2020: WRF-based dynamical downscaling of ERA5 reanalysis data for High Mountain Asia: Towards a new version of the High Asia Refined analysis. *Int. J. Climatol.*, **2020**, 1–20, https://doi.org/10.1002/joc.6686.

Wei, W., Y. Wu, S. Yang, and W. Zhou, 2019: Role of the South Asian high in the onset process of the Asian summer monsoon during spring-to-summer transition. *Atmosphere*, **10**, 239, https://doi.org/10.3390/atmos10050239.

Wen, Y., A. Behrangi, B. Lambrigtsen, and P.-E. Kirstetter, 2016: Evaluation and uncertainty estimation of the latest radar and satellite snowfall products using SNOTEL measurements over mountainous regions in western United States. *Remote Sens.*, **8**, 904, https://doi.org/10.3390/rs8110904.

Wu, R., 2017: Relationship between Indian and East Asian summer rainfall variations. *Adv. Atmos. Sci.*, **34**, 4–15, https://doi.org/10.1007/s00376-016-6216-6.

Xu, K., L. Zhong, Y. Ma, M. Zou, and Z. Huang, 2020: A study on the water vapor transport trend and water vapor source of the Tibetan Plateau. *Theor. Appl. Climatol.*, **140**, 1031–1042, https://doi.org/10.1007/s00704-020-03142-2.

Xu, R., F. Tian, L. Yang, H. Hu, H. Lu, and A. Hou, 2017: Ground validation of GPM IMERG and TRMM 3B42V7 rainfall products over southern Tibetan Plateau based on a high-density rain gauge network. *J. Geophys. Res. Atmos.*, **122**, 910–924, https://doi.org/10.1002/2016JD025418.

Xu, X., C. Lu, X. Shi, and S. Gao, 2008: World water tower: An atmospheric perspective. *Geophys. Res. Lett.*, **35**, L20815, https://doi.org/10.1029/2008GL035867.

Yanai, M., and T. Tomita, 1998: Seasonal and interannual variability of atmospheric heat sources and moisture sinks as determined from NCEP–NCAR reanalysis. *J. Climate*, **11**, 463–482, https://doi.org/10.1175/1520-0442(1998)011<0463:SAIVOA>2.0.CO;2.

——, and G.-X. Wu, 2006: Effects of the Tibetan Plateau. *The Asian Monsoon*, Springer Berlin Heidelberg, 513–549.

——, C. Li, and Z. Song, 1992: Seasonal heating of the Tibetan Plateau and its effects on the evolution of the Asian summer monsoon. *J. Meteor. Soc. Japan*, **70**, 319–351, https://doi.org/10.2151/jmsj1965.70.1B_319.

Yang, K., B. Ye, D. Zhou, B. Wu, T. Foken, J. Qin, and Z. Zhou, 2011: Response of hydrological cycle to recent climate changes in the Tibetan Plateau. *Climatic Change*, **109**, 517–534, https://doi.org/10.1007/s10584-011-0099-4.

Yao, T., and Coauthors, 2013: A review of climatic controls on δ^{18}O in precipitation over the Tibetan Plateau: Observations and simulations. *Rev. Geophys.*, **51**, 525–548, https://doi.org/10.1002/rog.20023.

——, and Coauthors, 2019: Recent Third Pole's rapid warming accompanies cryospheric melt and water cycle intensification and interactions between monsoon and environment: Multidisciplinary approach with observations, modeling, and analysis. *Bull. Amer. Meteor. Soc.*, **100**, 423–444, https://doi.org/10.1175/BAMS-D-17-0057.1.

Ye, D. Z., and G. X. Wu, 1998: The role of the heat source of the Tibetan Plateau in the general circulation. *Meteor. Atmos. Phys.*, **67**, 181–198, https://doi.org/10.1007/BF01277509.

Yeh, T.-C., 1957: The wind structure and heat balance in the lower troposphere over the Tibetan Plateau and its surroundings. *Acta Meteor. Sin.*, **28**, 108–121.

Yim, S.-Y., B. Wang, J. Liu, and Z. Wu, 2014: A comparison of regional monsoon variability using monsoon indices. *Climate Dyn.*, **43**, 1423–1437, https://doi.org/10.1007/s00382-013-1956-9.

You, Q., J. Min, W. Zhang, N. Pepin, and S. Kang, 2015: Comparison of multiple datasets with gridded precipitation observations over the Tibetan Plateau. *Climate Dyn.*, **45**, 791–806, https://doi.org/10.1007/s00382-014-2310-6.

Zhang, C., Q. Tang, and D. Chen, 2017: Recent changes in the moisture source of precipitation over the Tibetan Plateau. *J. Climate*, **30**, 1807–1819, https://doi.org/10.1175/JCLI-D-15-0842.1.

Zhang, F., 2019: Spatial pattern and seasonal variation of alkaline precipitation observed in the Gansu Province, NW China. *Environ. Earth Sci.*, **78**, 417, https://doi.org/10.1007/s12665-019-8442-6.

Zhang, P., Y. Liu, and B. He, 2016: Impact of East Asian summer monsoon heating on the interannual variation of the South Asian high. *J. Climate*, **29**, 159–173, https://doi.org/10.1175/JCLI-D-15-0118.1.

Zhang, R., D. Jiang, Z. Zhang, and E. Yu, 2015: The impact of regional uplift of the Tibetan Plateau on the Asian monsoon climate. *Palaeogeogr. Palaeoclimatol. Palaeoecol.*, **417**, 137–150, https://doi.org/10.1016/j.palaeo.2014.10.030.

Zhang, S., D. Wang, Z. Qin, Y. Zheng, and J. Guo, 2018: Assessment of the GPM and TRMM precipitation products using the rain gauge network over the Tibetan Plateau. *J. Meteor. Res.*, **32**, 324–336, https://doi.org/10.1007/s13351-018-7067-0.

Zhang, X., D. Chen, and T. Yao, 2018: Evaluation of circulation-type classifications with respect to temperature and precipitation variations in the central and eastern Tibetan Plateau. *Int. J. Climatol.*, **38**, 4938–4949, https://doi.org/10.1002/joc.5708.

Zhang, Z., J. C. L. Chan, and Y. Ding, 2004: Characteristics, evolution and mechanisms of the summer monsoon onset over Southeast Asia. *Int. J. Climatol.*, **24**, 1461–1482, https://doi.org/10.1002/joc.1082.

Zhou, F., R. Zhang, and J. Han, 2020: Influences of the East Asian summer rainfall on circumglobal teleconnection. *J. Climate*, **33**, 5213–5221, https://doi.org/10.1175/JCLI-D-19-0325.1.

Zhu, Y., and Y. Sang, 2018: Spatial variability in the seasonal distribution of precipitation on the Tibetan Plateau. *Prog. Geogr.*, **37**, 1533–1544, https://doi.org/10.18306/dlkxjz.2018.11.009.

——, and S. Yang, 2020: Evaluation of CMIP6 for historical temperature and precipitation over the Tibetan Plateau and its comparison with CMIP5. *Adv. Climate Change Res.*, **11**, 239–251, https://doi.org/10.1016/j.accre.2020.08.001.

——, Y. Sang, D. Chen, B. Sivakumar, and D. Li, 2020: Effects of the South Asian summer monsoon anomaly on interannual variations in precipitation over the south-central Tibetan Plateau. *Environ. Res. Lett.*, **15**, 124067, https://doi.org/10.1088/1748-9326/abc71b.